ORGANISATION EUROPÉENNE POUR LA RECHERCHE NUCLÉAIRE

CERN EUROPEAN ORGANIZATION FOR NUCLEAR RESEARCH

PRECISE MEASUREMENTS OF PARTICLE PRODUCTION
BY 400 GeV/c PROTONS ON BERYLLIUM TARGETS

H.W. Atherton, C. Bovet, N. Doble, G. von Holtey, L. Piemontese[*],
A. Placci, M. Placidi, D.E. Plane, M. Reinharz and E. Rossa

G E N E V A

1980

[*] On leave from the Istituto Nazionale di Fisica Nucleare, Sezione di
Trieste, Italy.

ABSTRACT

Results are given for beam composition and absolute production cross-sections in proton-beryllium collisions at 400 GeV/c. Measurements have been made on positive and negative particles at four momenta (60, 120, 200, and 300 GeV/c), two transverse momenta (0 and 500 MeV/c), and for three target lengths (100, 300, and 500 mm). Production cross-sections are derived from measurements on a short (40 mm) target.

CONTENTS

1. INTRODUCTION

In addition to the intrinsic interest of particle production measurements, a good knowledge of the production of secondary hadrons by 400 GeV/c protons striking beryllium targets is needed in order to calculate, with high precision, the shape of the CERN neutrino-beam spectra. In particular, a good measurement of the K/π ratio of production cross-sections at various energies and production angles is essential[1].

Precise measurements are difficult and time-consuming, so that the measurement of a dense set of points, closely spaced in energy and production angle, would require a long running-time.

In this exploratory work we aimed at measuring only a few points but with high precision. In Section 2 we describe the experimental apparatus and the measurement procedure; in Section 3 the data reduction, including the corrections applied to the data and the sources of error; and we give the results in Section 4.

2. THE EXPERIMENTAL METHOD

The measurements have been performed in the H2 beam[2] of the CERN Super Proton Synchrotron (SPS). A simplified drawing of the beam is given in Fig. 1. Absolute fluxes were counted in four scintillation counters, and beam composition was measured by two N-type CEDARs[3], which are the standard differential Čerenkov counters (built and operated by the SPS Division Experimental Areas Group) for particle identification in the 60-300 GeV/c region.
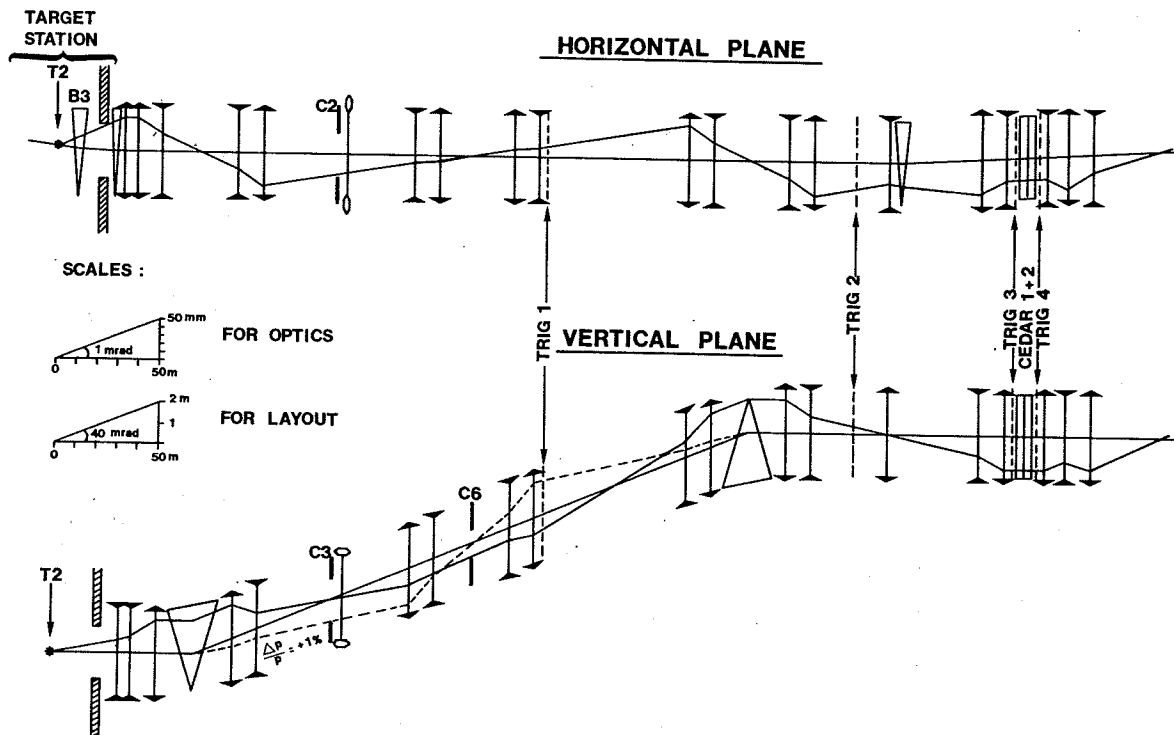

Fig. 1   Layout and optics of H2 beam

2.1 The apparatus

2.1.1 Beam optics and collimators

The H2 beam is a high-energy secondary hadron beam serving experiments in hall EHN 1 of the SPS North Experimental Area[2]. The optical structure of the beam in its high-resolution mode, as used for the measurements, is shown schematically in Fig. 1. The principal momentum analysis and recombination occur in the vertical plane, collimator C3 being used to define the momentum bite transmitted by the beam. Collimators C2 and C6 serve to define the horizontal and vertical angular acceptance of the beam. These collimators were always kept sufficiently closed so as to ensure that they determined the beam transmission and that particles within the transmitted phase space were not lost elsewhere.

The beam was rendered parallel to ≤ 0.02 mrad in both planes in order to allow efficient particle identification by Čerenkov counters CEDAR 1 and CEDAR 2. For this purpose the second-order contribution to the beam divergence at the CEDARs, due to cumulative chromatic aberration of the quadrupoles, was corrected in the horizontal plane by means of a sextupole acting at a position of vertical dispersion (adjacent to C3).

2.1.2 Selection of production angles

The layout of target station T2, from which two beams (H2 and H4) are derived, is shown schematically in Fig. 2. The direction of incidence of the primary proton beam onto the target is governed by magnets B1 and B2. Magnets B3 and B4 then serve to direct secondary particles of wanted sign, momentum, and production angle into the beam H2, whilst deviating the remaining primary beam (+400 GeV/c) onto the dump. The production angle of the H2 beam was varied by changing the strength of B3 and by correspondingly correcting B4 to put the beam back on axis. In this way symmetrical production angles on either side of zero were obtained (broken trajectories in Fig. 2).
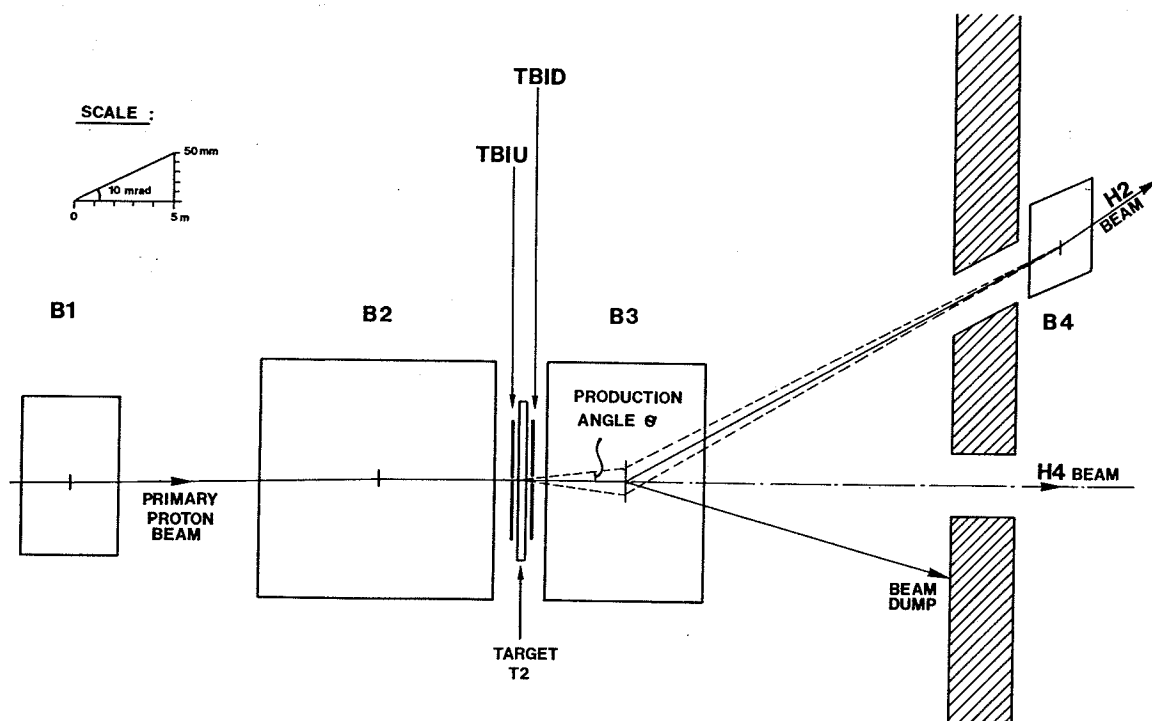

Fig. 2 Plan of target station T2

2.1.3 Targets

The actual production target consists of one of a series of beryllium plates, each of which may be brought into position so that the primary proton beam enters the plate along its median plane[4]. Five alternative target plates of dimensions listed in Table 1, and one empty position, have been used.

Table 1

List of targets

Length (in beam direction) (mm)	Width (horizontal) (mm)	Height (vertical) (mm)
500	160	2.0
300	160	2.0
300	160	1.5
100	160	2.0
40	160	2.0

2.1.4 Target box instrumentation

The target assembly is immediately preceded and succeeded by instrumentation boxes (TBIU upstream and TBID downstream, Fig. 2) containing Secondary Emission Monitors (SEM). These boxes may be moved laterally in the horizontal plane so as to follow the displacement of the primary beam caused by magnets B1 and B2 of the target station (Fig. 2). Each box contains a set of split foils (BSP-H, BSP-V) used for steering the primary beam onto the target in the horizontal and vertical planes, and a series of complete foils (BSI-U, in the upstream box, BSI-D in the downstream box) used to monitor the intensity of the primary beam. SEM profile scanners are also provided in the TBIU target monitor box. They consist of thin strips which can be scanned across the beam in steps as fine as 0.05 mm in both planes. The incident proton flux is given by the output of the BSI-U foil, which was specially calibrated[5] so as to provide an absolute measure of the protons entering the target. The ratio BSI-D/BSI-U, or "multiplicity", provides a record of the efficiency with which the primary beam strikes a target of given geometry.

2.1.5 Detectors

Four 3 mm thick scintillation counters, TR1 to TR4, counted the whole beam. Counters TR1 and TR2 were located at 233.5 m and 385.6 m from the target, respectively, and were separated by a dipole. Counters TR3 and TR4 were located at 459.6 m and 473.6 m from the target, straddling the two CEDARs. An N-type CEDAR[3] is a 6 m long differential Čerenkov counter filled with high-pressure (10 to 14 bar) helium, and equipped with an optical system which corrects the chromatic aberrations and focuses Čerenkov light, produced at an angle of 25.8 mrad, on a circular light-diaphragm (LD) of 20 cm diameter. The LD opening can be varied from 0 to 20 mm with a ±20 μm precision; the light is then transmitted through quartz windows onto eight photomultipliers. The beam hole of a CEDAR is a 10 cm diameter circle; with a wide-aperture LD, the average number of photoelectrons per photomultiplier ranges from 2.5 to 3.4, depending on the photomultiplier characteristics. In order to separate events due to stray particles hitting the photomultipliers of the CEDARs, a large scintillation counter (ANTI), with a 10 cm diameter hole, was placed just before each CEDAR.

From the signals coming from the different detectors, the following coincidences were formed and counted: TR1 × TR2 and TR3 × TR4 were used to count the total beam intensity; the latter, called TRIGGER, was also used in coincidence with the CEDARs as a strobe. The signals from the eight photomultipliers of a CEDAR were shaped to about 10 ns, and entered a NIM circuit which gave three coincidence signals: sixfold, sevenfold, eightfold. The coincidences 6(7,8)-fold × $\overline{ANTI}$ × TRIGGER were made and counted together with the trigger. The sixfold coincidence has a very high efficiency, while the eightfold one has lower efficiency but better resolution.

In order to make a precise measurement of the beam direction and divergences in the magnet-free region where the CEDARs were located, a pair of FIlament SCanners (FISC)[6] were installed at the beginning and another pair at the end of this straight beam section, 15 m downstream.

A FISC is a thin scintillator strip, 10 cm long and 0.2 mm wide, viewed by two photomultipliers in coincidence. The scintillator can be moved in a direction normal to the beam, and two FISCs are used as a pair to provide scans in the horizontal and vertical planes, respectively.

2.2 Measurement procedure

2.2.1 Beam setting and measurement of absolute fluxes

In general, the required production angle at any given momentum was selected by setting the third target station magnet (B3 of Fig. 2) to the calculated value, and scanning the first septum magnet of the beam line (B4 of Fig. 2) to put the beam on the required axis. For non-zero production angle, both signs of production angle could be selected and the fluxes measured. The equality of these two measurements gave an estimate of the accuracy when selecting the production angle. To determine the zero-degree production angle, a scan of flux versus production angle was made by varying the angle of the incoming protons onto the target with B1 + B2. The maximum of such scans (sensitive only at 200 and 300 GeV/c) was taken as the zero-degree production angle, and showed a misalignment of 0.23 mrad to the theoretical geometrically aligned zero angle. This misalignment was corrected during the measurements by maintaining small currents in B1 and B2.

The proton beam was continuously monitored in intensity and frequently in size, angle of strike onto the target, and angular divergence.

The spot size was measured by using the SEM profile scanners. Analysis of many scans during the whole run allowed the beam "radius" to be extracted at any time. This radius was very stable during the entire measurement period.

The targets are very large horizontally and small (2 mm) vertically (see Section 2.1.3). Hence only the vertical spot size was important in evaluating the fraction of the incident proton beam which struck the target. An independent measurement of this fraction (besides the profile scans) was made by measuring the relative fluxes from two targets of different vertical sizes (1.5 and 2.0 mm) but with identical lengths and horizontal size. Assuming the beam to be Gaussian in the vertical plane (as was demonstrated to be the case by the profile scans), the ratio of the two fluxes allowed the beam width to be calculated. The above two independent measurements agreed to about 0.5% and gave the fraction of incident protons hitting the target to be 97 ± 1%.

After setting up the target station and beam steering, the beam was adjusted, using the FISC counters, to be parallel at the CEDAR detectors.

In each plane, profiles were obtained by scanning the downstream FISC in coincidence with the upstream FISC, the latter being fixed at each of several positions across the beam. A comparison between the displacements of the centres of the profiles and the displacements of the fixed FISC provided a measure of the inclination of the beam phase-space ellipse to a precision of $\pm 2 \times 10^{-4}$ mrad/mm. Accordingly this ellipse could be rotated to be upright, i.e. the beam was rendered "parallel", in both planes, by iterative adjustments to the strengths of the two quadrupoles immediately preceding the CEDARs. The widths of the FISC coincidence profiles provided a measure of the intrinsic parallelism due to the emittance of the beam, and hence allowed the sextupole correction for chromatic aberration to be checked.

Having checked the steering and focusing of the beam, the total yields for the given acceptance were measured for each target head, including the empty target head position. Each head was successively moved into position in the proton beam, and the rates of the trigger pair coincidences were recorded for 15 SPS pulses.

For each pulse we also recorded the readings of the SEM intensity foils of the target box, both upstream and downstream, and of the asymmetry foils (to show pulse-to-pulse variations of steering). These measurements allowed the proton beam stability to be monitored during the data taking. The counting rates were kept below 10^6 particles per second.

2.2.2 *Particle identification*

Once the beam was tuned, TR1 and TR2 were moved out of the beam line and the two CEDARs were aligned. The light-diaphragms were then set at a value of maximum aperture compatible with good π-K separation. Figures 3a and 3b show pressure scans of a CEDAR at 200 and 300 GeV/c.
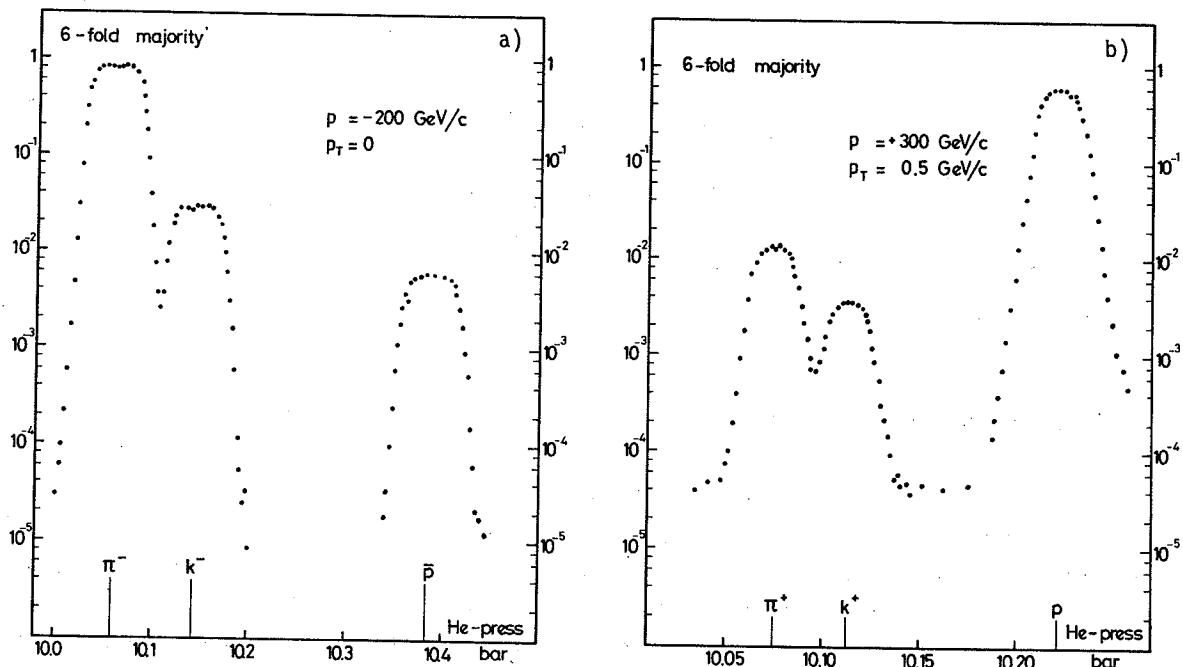

Fig. 3 Examples of CEDAR pressure scans

The measurements were done by counting TRIGGER counts and computing the ratio

$$\frac{6(7,8)\text{-fold} \times \overline{\text{ANTI}} \times \text{TRIGGER}}{\text{TRIGGER}}$$

(see Section 2.1.5) for each pressure setting.

Instead of making a complete pressure scan for each beam condition, we set the pressure of the CEDARs on the peak of a particle, waited for the settling of the gas (the turbulence in a CEDAR has a negative effect on efficiency at small diaphragm settings), and then measured the fraction of this particle with a local scan around the top of the peak. The same operation was repeated for the two other targets. The CEDAR pressure was then moved to another particle peak, and the whole operation was repeated.

At 60 GeV/c, where the CEDAR resolution allows a separation of pions and electrons, two measurements have been made in the e-π region: the e + π beam content has been measured with a wide diaphragm setting (2.5 mm) and the e/π ratio with a small diaphragm (0.53 mm). A typical e-π separation scan is shown in Fig. 4.
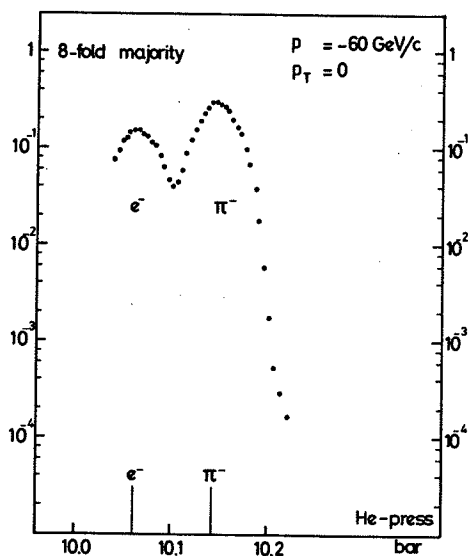
Fig. 4 Typical e-π separation scan

3. DATA PROCESSING AND EXPERIMENTAL ERRORS

3.1 Beam parameters

3.1.1 Beam momentum

The determination of the momentum of the secondary beam relies on knowing the excitation curves of the bending magnets. These are known with an error which is estimated to be < 1%. We have a consistency check on this 1% figure, as follows. Different detection coils and reference magnets were used to measure the characteristics of bending magnets and quadrupoles, with the result that we have independent and different systematic errors for these two types of beam transport element. This could give rise to a situation where the beam is well steered (i.e. bending magnets set correctly) but not well focused. With one exception we found that with a well-steered beam, the quadrupoles had to be tuned to values differing

by much less than 1% from their calculated values. The exception occurred at -300 GeV/c, where a global correction of 0.8% to all the beam quadrupoles was required to give a beam matched to the computed conditions at the CEDAR. We therefore conclude that our uncertainties on the quoted momenta are equal to 1% or less.

3.1.2 *Production angles*

Production angles were selected according to the procedure described in Section 2.1.2, and the zero degree line of the primary proton beam was measured as described in Section 2.2.1.

Several factors had to be taken into consideration when determining the transverse momentum acceptance Δp_T: the horizontal and vertical beam acceptance, and the divergence of the incident proton beam. The beam angular acceptances are known and determined by collimator openings. The proton beam divergence was measured in both planes before every flux measurement. It turns out that the horizontal divergence of the proton beam, measured as $\sigma = 0.4$ mrad, dominates. The transverse momentum acceptance is thus given by

$$\Delta p_T \text{ MeV/c} = 0.4 \times p \; ,$$

where p is the secondary beam momentum in GeV/c.

3.1.3 *Equivalent target length*

The lengths of the beryllium targets used are well known; however, even with the target moved out, some flux was still measured in the beam line. This flux was due to the interactions of the proton beam with the air in the target station ($\simeq$ 3 m long), the vacuum windows, and the SEM foils themselves. Added together they represent about 0.6% of an interaction length. At each data-taking point, the empty target position flux was also recorded in order to subtract its effect.

The measured values of this target-out flux compared to target-in were constant over the entire run, and this corresponds to 2.2 ± 0.1 mm of Be, i.e. 0.55% of an interaction length, as expected. Thus this represents a correction of 5% to the 40 mm target data but of only 1% to the 500 mm target data. The accuracy of estimating this correction introduces an error on the cross-sections of < 0.2%.

3.1.4 *Acceptances*

The accuracy of the total beam acceptance relies on the knowledge of the gaps between the jaws of the beam-defining collimators (C2, C3, C6). Each jaw of the collimator is independently variable in position, and this position was measured with a linear resistive transducer attached to the jaw. The transducer scale has been measured in the laboratory so that the error on the measured gap is $\simeq$ 0.15 mm. What was not known was the offset of the jaw relative to the beam axis, but this was measured using the beam itself. With the beam set at -200 GeV/c and 0°, the beam flux was measured as a function of one collimator opening, the other two collimators remaining fixed. The result was, as expected, a linear increase of flux with opening until the opening exceeded the calculated maximum beam acceptance. The intercept of the line was determined using a maximum likelihood fit to the points. This offset could be determined to $\simeq$ 0.1 mm, and only C3 was found to have such an offset not consistent with zero. It should be noted that this measurement also gave a direct measurement of edge effect (beam entering the collimator and scattering back into the beam), as it would show up as an apparent offset in the measurement.

The final error achieved on jaw opening is estimated as 0.2 mm, which represents a typical error of between 1 and 4% on the beam acceptance.

As these collimators are inside the quadrupole structure of the beam line, the acceptance also relies on the accuracy of the beam tuning. This was checked mainly by the corrections necessary for the parallelism at the CEDARs (see Section 2.1). Feeding these variations into a transfer matrix element calculation contributes a 3.5% uncertainty on the knowledge of the total beam acceptance.

3.2 Absolute fluxes

3.2.1 Secondary emission foil calibration

The calibration factor or sensitivity of the SEM foil was measured in a separate experiment by an activation foil technique. Reference 5 contains full details, and the error on this calibration at the time of measurement was 1.8% (Table 6 of Ref. 5).

Unfortunately it was found that this monitor showed a strong drift (10%) over a period of days during our running. This drift was monitored at frequent intervals by cross-comparison of signals from the foils in front of and behind the target with and without the targets in place, and by monitoring beam position and profiles to be constant.

By repeating measurements with the beam line set to identical settings at several points during the run and at several energies, it was possible to show that apparent flux variations were proportional to inferred variations in the upstream (TBIU) foil.

This TBIU foil was a new one installed just before our run, whereas the downstream TBID foils were old ones that had already been used and irradiated for a few months. From experience with such foils [see Agoritsas and Witkover[7] and Dieperink[8] for example] strong variations in new foils are to be expected, whereas old foils are more stable (under identical beam conditions) and have only "small" variations, on the time scale of a few days.

Owing to the above effects a systematic error of 3% must be imposed in addition to the apparent calibration error.

3.2.2 Dead-time of counters

Counting losses due to dead-time of the coincidences (TR1 × TR2) and (TR3 × TR4) have been corrected for. To keep losses down, the beam intensity during the flux measurements was adjusted, in the limits of keeping a reasonably large collimator opening in order to reduce the error on acceptance, to between 10^5 and 10^6 particles/burst at the triggers.

The dead-time of the two coincidences has been measured on the oscilloscope, while the effective spill-time of the slow ejection to the North Area has been obtained from measurements made in the neighbouring beam line by the NA3 Experiment and logged over the period of our running. With these data it has been possible to evaluate the relative counting losses (in percent) of the two signals, which are, of course, proportional to the beam intensity. At a beam intensity of 10^6 particles/burst, they were 2.8% for TR1 × TR2 and 3.9% for TR3 × TR4. The uncertainty of these corrections is estimated to be 20%.

3.2.3 Compatibility of counting rates

As mentioned in Section 2.1.5, the flux was measured with two independent trigger pairs (see Fig. 1). As they are at different positions in the beam line, any difference in counting

rate should be due (after unfolding dead-time losses) only to absorption and decay between these two counting positions.

For +300 GeV/c the beam is 99% protons and only absorption must be considered. The counting-rate difference of 2.4% measured in this case is entirely consistent with the amount of absorbing material in the beam line between the two positions and is therefore taken as an absorption reference.

Using this information, it is possible to calculate the expected rate difference between the two trigger coincidences, which is due to decay between the two positions, at other momenta. The measured difference varies from 2.4% at -300 GeV/c to 6.8% for +60 GeV/c and is consistent, to $\simeq$ 0.5%, with the theoretical changes expected from decay.

As these two trigger systems pass through entirely different electronic chains and are separated physically by more than 100 m, the agreement found gives confidence in the stability of TR3 × TR4 used for the flux measurements.

3.2.4 *Errors*

Measuring absolute fluxes over 15 SPS bursts generally gave a statistical accuracy of < 0.5% on the mean flux per proton. This error, coming entirely from the SEM intensity foil, is due to the finite resolution of the ADC used to convert the measured analog SEM voltage to digital form.

The total measurement error is dominated by the following three systematic errors:

  i) SEM calibration, see Section 3.2.1 $\simeq$ 5%

 ii) errors in beam optics, see Section 3.1.4 $\simeq$ 4%

iii) collimator opening uncertainty $\simeq$ 1-4%.

All other corrections are of the order of or less than 1%.

3.3 Particle ratios

A typical output of a CEDAR measurement is shown in Table 2: about 10 measurements were taken whilst scanning the CEDAR pressure over the peak of the particle being measured.

The light diaphragm was set to give good π-K separation even with the sixfold coincidence. As the sevenfold and eightfold coincidences have lower efficiency and are therefore more affected by errors due to slight variations of efficiency in time, the sixfold data have been used in measuring particle ratios. However, the e/π ratio at 60 GeV/c has been calculated by processing the eightfold data, as in this particular case the sixfold and sevenfold did not have sufficient separation.

The sixfold rates on the pressure peaks have been averaged over the measured points, and the r.m.s. error evaluated and taken as the statistical error. Once this has been done for p's, K's and π's + e's, the relative fractions have been added to obtain the CEDAR measured efficiency. The efficiencies can then be compared for different beam conditions (i.e. different target or production angles), at the same energy and light diaphragm setting, so as to have an idea of the influence of local variations of efficiency on the experimental error. Measured efficiencies and their fluctuations are given in Table 3.

Table 2

Example of CEDAR pressure scan print-out

```
CEDAR# 2 IN BEAM H2: SCAN FROM 10.0396 TO 10.031 BAR; STEP=  -.53 MBAR
L D=   053 MM; MOMENTUM: 340    GEV/C                1980-03-09-12:46:36

   PRESS    TRIG    NPE/PM    R    --------MAJORITIES-------  CYCLE MEAS
   [BAR]                           6-FOLD    7-FOLD   8-FOLD    #     #

  10.0396  4.44E6   .93   1.03   7.12E-4  2.29E-4  3.78E-5    4    1
  10.0386  4.30E6   .96   1.01   7.50E-4  2.60E-4  4.39E-5    4    2
  10.0379  4.42E6  1.00    .99   7.91E-4  2.99E-4  5.26E-5    4    3
  10.0373  4.48E6  1.02    .99   8.46E-4  3.28E-4  5.93E-5    4    4
  10.0366  4.49E6  1.13   1.03   8.58E-4  3.47E-4  7.32E-5    4    5
  10.0359  4.50E6  1.15   1.04   8.66E-4  3.58E-4  7.65E-5    4    6
  10.0352  4.49E6  1.10    .99   8.85E-4  3.73E-4  7.49E-5    4    7
  10.0346  4.42E6  1.16   1.06   8.63E-4  3.39E-4  7.61E-5    4    8
  10.0336  4.46E6  1.14   1.04   8.12E-4  3.26E-4  7.05E-5    4    9
  10.0332  4.48E6  1.12   1.07   7.82E-4  2.91E-4  6.22E-5    4   10
  10.0326  4.51E6  1.06   1.03   7.39E-4  2.75E-4  5.38E-5    4   11
  10.0315  4.45E6   .93   1.01   6.69E-4  2.24E-4  3.67E-5    4   12
  10.0309  4.47E6   .86   1.02   6.01E-4  1.80E-4  2.65E-5    4   13
```

Table 3

Efficiency of CEDARs

Energy, polarity (GeV/c)	p_T (GeV/c)	C1			C2		
		LD (mm)	Efficiency (%)	Number of points	LD (mm)	Efficiency (%)	Number of points
-60	0	0.62	85.2 ± 0.6	3	0.62	66.6 ± 0.6	3
	0.5	2.52	96.6 ± 0.3	3	2.52	93.7 ± 0.15	3
+60	0 0.5	2.52	96.9 ± 0.3	6	2.52	94.0 ± 0.5	6
-120	0 0.3 0.5	1.24	95.7 ± 0.18	9	1.24	92.5 ± 0.23	9
+120	0 0.3 0.5	1.24	94.85 ± 0.27	9	1.24	91.13 ± 0.54	9
-200	0	0.23	80.0 ± 1.8	3	0.23	69.5 ± 1.5	3
	0.5	0.23	66.2 ± 2.0	3	0.23	71.8 ± 3.3	3
+200	0 0.5	0.31	86.71 ± 1.3	3	0.25	78.34 ± 0.5	3
					0.31	77.6 ± 1.0	3
-300	0	0.13	58.2 ± 0.3	3	0.13	50.6 ± 0.4	3
	0.5	0.13	56.2 ± 1.5	3	0.13	48.9 ± 1.5	3
+300	0.5	0.13	64.5 ± 1.0	3	0.13	56.5 ± 0.5	3

The measured fractions have then been divided by their own efficiency to get the normalized rates. Only in the case of particularly bad measurements has another procedure been followed (see Section 3.3.3). The normalized rates have then been corrected for the following effects.

3.3.1 Background

CEDARs have a constant background level between particle peaks, which is intensity-dependent but always smaller than 10^{-4}. The background, which is significant only at 300 GeV/c when the production of minority particles drops to minute values, has been subtracted from the data. An error equal to the correction has been assumed (always smaller than 5%).

3.3.2 Limited rejection

The rejection of pions under the kaon peak has been studied at length by putting CEDAR 1 and CEDAR 2 in coincidence and scanning the masses with one of them when the other is sitting on the pion peak.

The contamination of the kaons by pions, due to limited rejection, is significant only at 300 GeV/c negative particles, and the correction applied is 1% for CEDAR 1 and 2% for CEDAR 2. The error in the correction has been taken equal to the correction itself.

3.3.3 CEDAR efficiency

At some beam conditions, the beam consists of more than 90% of one type of hadron (e.g. 99% π^- at 300 GeV/c).

In such a case, the sum of measured rates reflects the efficiency only during the measurement of the abundant particles. In certain cases, therefore, the average CEDAR efficiency has been calculated over the different targets and/or angles, and then the measured fractions of rare particles have been divided by this average efficiency. The rest of the beam has been assigned to the most frequent particles.

3.3.4 Electrons in the beam

At 60 GeV/c the e/π ratio has been measured with the CEDARs. The peaks being very sharp, it has not been possible to average values over a few points. The peak value has been taken for the rate, and a 4% relative error in the measured e/π ratio has been assumed. It is worth remarking that at 0 mrad angle with the long target, where the e/π ratio is typically 40-50%, this is the largest contribution to the π flux error and also the K/π error.

At 120 GeV/c the CEDAR can no longer separate electrons from pions. A measurement of e contamination in the beam has been made with negative particles at 0 mrad production angle, by inserting a 3 mm thick sheet of lead next to TR1. The electrons lose energy by bremsstrahlung in the lead and are lost in the subsequent bending magnets. By measuring the loss of counts with and without the lead in the beam, for the 40, 100, 300, and 500 mm targets, it has been possible to evaluate the electron contents in the beam. These data and those at 60 GeV/c have been used to check the reliability of a Hagedorn-Ranft + beam transport program which calculates the e/π ratios. This program has then been used to calculate the $e^\pm$ content for other conditions at 120 GeV/c. The $e^\pm$ content for other angles is < 5%, and the relative error has been taken as 20%, the maximum difference between the program and the measurements described above. For energies $\geq$ 200 GeV/c the electrons lose too much energy in the bending magnets through synchrotron radiation, and are swept away before the CEDARs.

3.3.5 *Muons in the beam*

Muons from pions and kaons decaying along the beam and hitting TR3 and TR4 can influence the measurements, either -- if counted by CEDARs -- by simulating a pion, or -- if not counted by CEDARs because their trajectory is too skew -- by simulating CEDAR inefficiency.

The fraction of μ's in the beam, both inside and outside the CEDAR angular acceptance, has been computed at each energy with a Monte Carlo program.

Data have been corrected for these muons, and the error in μ evaluation has been taken into account. The maximum amount of this correction was 3%.

3.3.6 *Decays and absorption between CEDARs and averaging data from CEDAR 1 and CEDAR 2*

Before averaging the data of the two CEDARs, one must refer them to the same physical conditions.

CEDAR 2 data have been corrected for decays after CEDAR 1 and absorption between CEDAR 1 and CEDAR 2. The net effect is that p's ($\bar{p}$'s) are absorbed more than π's and K's. Proton rates measured by CEDAR 2 have therefore been increased by 1%, while π and K rates are unchanged. Decay corrections are negligible, apart from those for 60 GeV/c kaons (1.6%).

After all previous corrections were applied, the data from the two CEDARs were averaged (when both were present) with, in general, equal weights.

3.3.7 *Decays along the beam line*

The particle rates have been corrected for decays of π's and K's over 461.5 m, which is the distance between the production target and the point in CEDAR 1 where enough light has been emitted to give 50% efficiency (sixfold).

3.3.8 *Absorption in materials along the beam line*

To evaluate the particle losses due to interactions with the material along the beam line, we have taken the absorption cross-sections measured at Fermilab by Carroll et al.[9]. The quoted cross-sections have been (somewhat arbitrarily) increased by 15% in order to take into account the elastic and quasi-elastic cross-sections.

The losses along the beam line until TR3 range from 1.1% to 1.9% according to the particle type; the loss in one CEDAR ranges from 1.4% to 3.1% according to particle type and gas pressure.

The interactions in the CEDARs have been separated into three categories:

a)   secondaries do not hit TR4 (no trigger);

b)   secondaries hit TR4 -- neither CEDAR 1 nor CEDAR 2 give a signal;

c)   secondaries hit TR4 -- CEDAR 1 gives a signal and CEDAR 2 does not.

The total interaction probability has been split into these three categories according to energy and to partial cross-sections given in Ref. 9. It turns out that interactions of types (b) and (c) are well taken care of by just increasing the p ($\bar{p}$) rate in CEDAR 2 by 1% before averaging it with CEDAR 1 (see Section 3.3.6). The largest effect is due to type (a) interactions. Data have been corrected for these losses, and the error on the correction has been estimated to be 30% of the correction.

4. RESULTS AND DISCUSSION

4.1 Particle contents

The whole experiment, including the first setting up of the beam, the tuning and debugging of detectors and electronics, plus the systematic measurements, took about 10 days. Because of the limited time available, we could not repeat some of the measurements where the best possible precision had not been reached. In particular, the 200 GeV/c data, the 60 GeV/c negatives at 0 mrad, and 60 GeV/c positives at 8.33 mrad suffer from this defect.

Table 4 shows the particle composition at the end of 100, 300, and 500 mm long beryllium targets. Only $\pi^{\pm}$'s, $K^{\pm}$'s, p's, $\bar{p}$'s, and $e^{\pm}$'s where appropriate, reach the CEDARs to be measured: these have been taken to make up 100% of the beam leaving the target. The contribution of μ's, which are not produced in the target, has been subtracted.

At 200 and 300 GeV/c, the $e^{\pm}$'s produced from the target undergo such strong synchrotron radiation in the bending magnets that they are lost from the beam and do not reach the CEDARs.

Because of the necessity to make a clean dump of the unused incident proton beam, it was not possible to make measurements at $p_T = 0$ for 300 GeV/c positives.

The strong variation of the $e^{\pm}$ content with p_T, compared with that of hadrons, is qualitatively easy to understand as being due to the cascade process

$$\pi^0 \to \gamma\gamma \qquad \text{in the target.}$$
$$\qquad\quad \hookrightarrow \gamma \to e^+ e^-$$
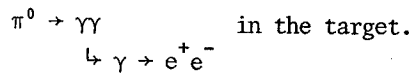
Their production is governed by the integral of π^0's with energy higher than the energy considered *at a fixed angle* of production. Figure 5 shows π^0 production [taken $= \frac{1}{2}(\pi^+ + \pi^-)$] at angles of 0, 4.17 and 8.33 mrad, as a function of secondary momentum, and shows the much larger momentum range contributing to the zero-angle integral rather than to the non-zero angles.

Fig. 5
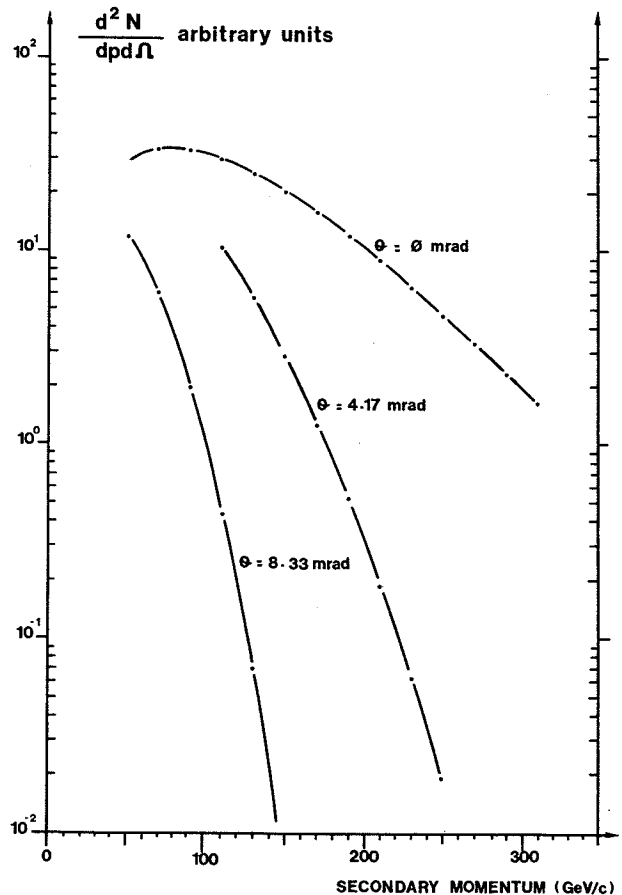Production of π^0 as a function of secondary momentum at three fixed angles

Table 4

Particle contents, in percent, of the beam leaving the beryllium production target

p (GeV/c)	p_T (MeV/c)	Target length (mm)	e⁻	π⁻	K⁻	p̄	e⁺	π⁺	K⁺	p
60	0	100	11.2 ± 0.3	79.3 ± 1.0	6.4 ± 0.2	3.1 ± 0.2	7.1 ± 0.2	69.7 ± 0.7	7.4 ± 0.1	15.8 ± 0.3
		300	22.0 ± 0.7	69.2 ± 1.0	6.2 ± 0.2	2.5 ± 0.1	14.4 ± 0.4	63.3 ± 0.7	6.93 ± 0.07	15.4 ± 0.3
		500	28.2 ± 0.8	64.2 ± 1.2	5.5 ± 0.2	2.1 ± 0.1	19.2 ± 0.6	58.9 ± 0.8	6.69 ± 0.09	15.2 ± 0.3
	500	100	1.83 ± 0.05	84.9 ± 0.8	8.71 ± 0.11	4.63 ± 0.08	0.99 ± 0.07	67.8 ± 0.9	9.5 ± 0.2	21.7 ± 0.5
		300	3.57 ± 0.11	83.4 ± 0.8	8.84 ± 0.11	4.23 ± 0.07	1.91 ± 0.13	65.6 ± 0.9	9.8 ± 0.2	22.7 ± 0.5
		500	4.63 ± 0.14	82.5 ± 0.8	9.06 ± 0.12	3.83 ± 0.07	2.33 ± 0.16	64.6 ± 0.8	9.7 ± 0.2	23.4 ± 0.6
120	0	100	2.8 ± 0.7	89.5 ± 1.1	5.87 ± 0.07	1.86 ± 0.03	1.1 ± 0.2	57.6 ± 0.7	4.55 ± 0.05	36.7 ± 0.6
		300	8.0 ± 0.8	84.6 ± 1.1	5.79 ± 0.07	1.64 ± 0.02	2.8 ± 0.6	55.9 ± 0.9	4.69 ± 0.06	36.7 ± 0.5
		500	9.1 ± 0.9	83.5 ± 1.2	5.87 ± 0.07	1.49 ± 0.02	3.9 ± 0.8	54.5 ± 1.1	4.80 ± 0.06	36.7 ± 0.6
	300	100	1.7 ± 0.3	89.4 ± 0.7	6.81 ± 0.08	2.16 ± 0.03	0.5 ± 0.1	49.1 ± 0.6	5.80 ± 0.07	44.6 ± 0.7
		300	4.3 ± 0.9	86.8 ± 1.0	6.90 ± 0.08	1.95 ± 0.03	1.3 ± 0.3	48.3 ± 0.6	5.82 ± 0.07	44.6 ± 0.7
		500	5.2 ± 1.0	86.2 ± 1.2	6.92 ± 0.08	1.76 ± 0.03	1.6 ± 0.3	47.9 ± 0.7	6.05 ± 0.07	44.5 ± 0.7
	500	100	1.1 ± 0.2	89.2 ± 0.3	7.13 ± 0.09	2.58 ± 0.04	0.3 ± 0.1	43.6 ± 0.5	6.69 ± 0.08	49.5 ± 0.7
		300	2.6 ± 0.5	87.8 ± 0.8	7.23 ± 0.09	2.35 ± 0.04	0.7 ± 0.2	43.0 ± 0.5	6.78 ± 0.08	49.5 ± 0.7
		500	3.7 ± 0.7	86.7 ± 1.0	7.40 ± 0.09	2.13 ± 0.03	1.1 ± 0.2	42.8 ± 0.5	7.02 ± 0.08	49.0 ± 0.7
200	0	100	- (a)	95.0 ± 0.6	4.30 ± 0.13	0.66 ± 0.03	- (a)	21.0 ± 0.6	2.49 ± 0.10	76.5 ± 0.5
		300	-	95.0 ± 0.6	4.33 ± 0.13	0.60 ± 0.02	-	20.8 ± 0.6	2.55 ± 0.10	76.6 ± 0.5
		500	-	95.0 ± 0.6	4.44 ± 0.13	0.55 ± 0.02	-	21.8 ± 0.7	2.78 ± 0.11	75.4 ± 0.5
	500	100	-	94.2 ± 0.6	5.05 ± 0.20	0.76 ± 0.03	-	16.4 ± 0.5	3.12 ± 0.09	80.4 ± 1.6
		300	-	94.1 ± 0.6	5.21 ± 0.21	0.69 ± 0.03	-	17.1 ± 0.5	3.28 ± 0.10	79.6 ± 1.0
		500	-	94.3 ± 0.6	5.15 ± 0.21	0.60 ± 0.02	-	17.5 ± 0.5	3.44 ± 0.10	79.0 ± 0.9
300	0	100	-	98.9 ± 0.4	1.04 ± 0.02	0.047 ± 0.002	-	- (b)	-	-
		300	-	98.9 ± 0.4	1.10 ± 0.02	0.046 ± 0.002	-	-	-	-
		500	-	98.8 ± 0.4	1.13 ± 0.02	0.042 ± 0.002	-	-	-	-
	500	100	-	98.8 ± 0.4	1.17 ± 0.04	0.046 ± 0.002	-	2.03 ± 0.04	0.617 ± 0.012	97.3 ± 0.5
		300	-	98.8 ± 0.4	1.20 ± 0.04	0.048 ± 0.002	-	2.09 ± 0.04	0.638 ± 0.019	97.3 ± 0.5
		500	-	98.8 ± 0.4	1.19 ± 0.04	0.041 ± 0.002	-	2.01 ± 0.04	0.641 ± 0.012	97.3 ± 0.5

Note:

a) For $p \geq 200$ GeV/c the $e^\pm$'s produced in the target are lost before the CEDARs owing to synchrotron radiation in the bending magnets.

b) 300 GeV/c, $p_T = 0$ positives were not measured.

4.1.1 *Particle ratios*

Table 5 shows the e/π, K/π, and p/π ratios. The errors are sometimes smaller than would be derived from Table 4, as they are only relative measurements which are not subject to all the systematic errors. Figure 6 shows them graphically as a function of secondary momentum
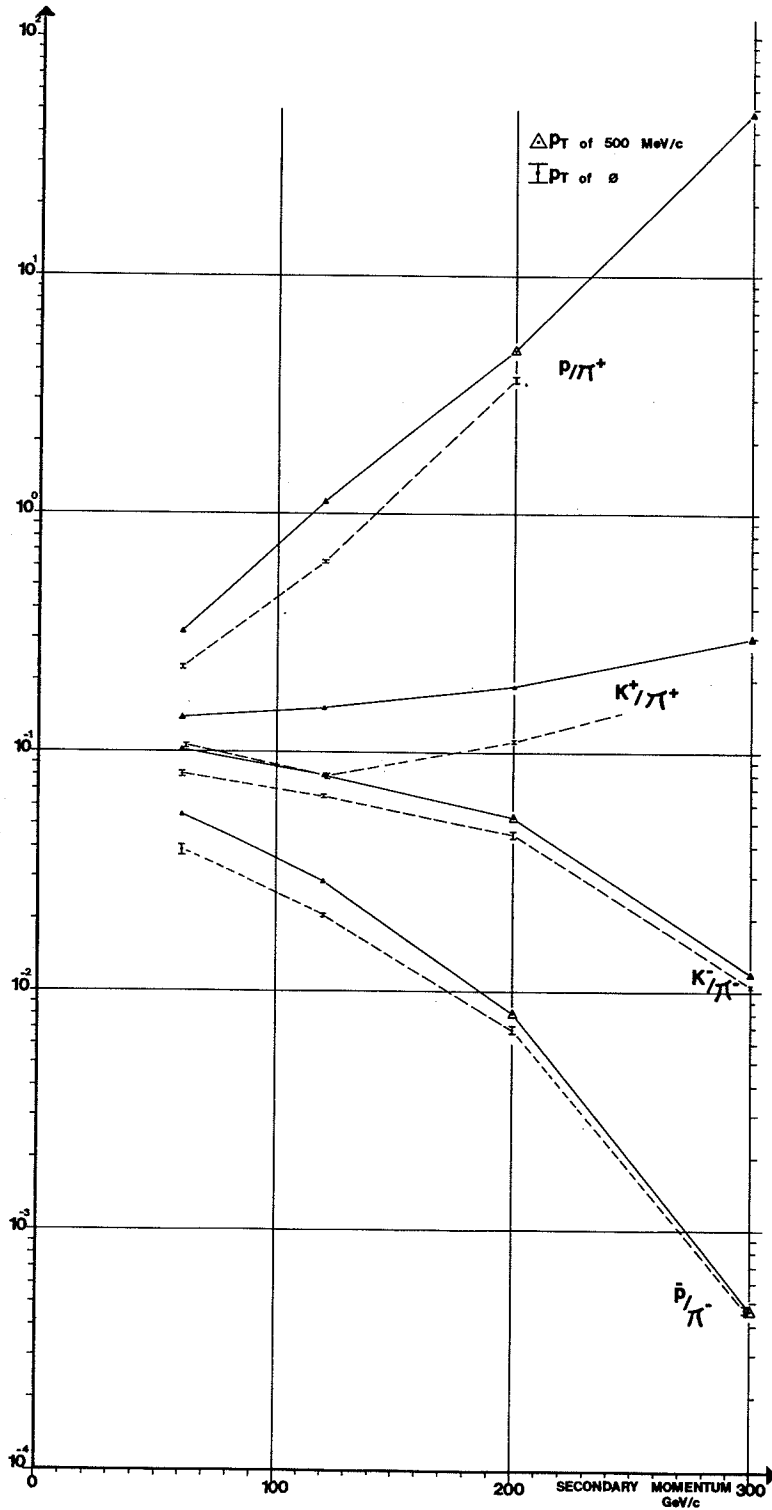

Fig. 6 Particle ratios as a function of secondary momentum from a 100 mm Be target

Table 5

Particle ratios in percent

p (GeV/c)	p_T (MeV/c)	Target length (mm)	e^-/π^-	K^-/π^-	$\bar{p}/\pi^-$	e^+/π^+	K^+/π^+	p/π^+
60	0	100	14.1 ± 0.4	8.09 ±0.24	3.88 ±0.19	10.1 ± 0.3	10.58 ± 0.11	22.7 ± 0.4
		300	31.8 ± 0.9	8.97 ±0.27	3.64 ±0.18	22.8 ± 0.7	10.96 ± 0.13	24.3 ± 0.4
		500	44.0 ± 1.7	8.54 ±0.34	3.34 ±0.20	32.6 ± 1.0	11.35 ± 0.11	25.8 ± 0.4
	500	100	2.16 ± 0.07	10.26 ±0.10	5.46 ±0.06	1.46± 0.10	14.0 ± 0.3	32.1 ± 0.6
		300	4.28 ± 0.13	10.61 ±0.11	5.08 ±0.05	2.90± 0.20	14.9 ± 0.3	34.6 ± 0.7
		500	5.61 ± 0.17	10.98 ±0.11	4.65 ±0.05	3.62± 0.25	15.1 ± 0.3	36.2 ± 0.7
120	0	100	3.2 ± 0.8	6.56 ±0.09	2.08 ±0.03	2.0 ± 0.4	7.91 ± 0.12	63.8 ± 1.0
		300	9.4 ± 0.9	6.84 ±0.10	1.94 ±0.03	5.0 ± 1.0	8.38 ± 0.15	65.6 ± 1.2
		500	10.9 ± 1.1	7.03 ±0.12	1.78 ±0.03	7.2 ± 1.4	8.80 ± 0.19	67.4 ± 1.9
	300	100	1.9 ± 0.4	7.54 ±0.08	2.40 ±0.02	1.1 ± 0.2	11.81 ± 0.17	90.7 ± 1.4
		300	5.0 ± 1.0	7.95 ±0.12	2.25 ±0.03	2.8 ± 0.6	12.06 ± 0.17	92.3 ± 1.4
		500	6.0 ± 1.2	8.03 ±0.14	2.04 ±0.04	3.3 ± 0.8	12.64 ± 0.22	93.0 ± 1.7
	500	100	1.2 ± 0.4	7.99 ±0.08	2.89 ±0.03	0.7 ± 0.2	15.35 ± 0.21	113.5 ± 1.7
		300	2.9 ± 0.6	8.24 ±0.09	2.67 ±0.03	1.7 ± 0.3	15.78 ± 0.22	115.3 ± 1.7
		500	4.3 ± 0.9	8.53 ±0.12	2.46 ±0.04	2.6 ± 0.5	16.39 ± 0.23	114.5 ± 1.7
200	0	100	(a)	4.52 ±0.14	0.692 ±0.028	(a)	11.9 ± 0.6	365 ± 11
		300		4.56 ±0.14	0.630 ±0.025		12.3 ± 0.6	368 ± 11
		500		4.67 ±0.14	0.577 ±0.023		12.7 ± 0.6	345 ± 10
	500	100		5.36 ±0.21	0.811 ±0.032		19.0 ± 1.0	490 ± 20
		300		5.54 ±0.22	0.734 ±0.031		19.1 ± 1.0	465 ± 14
		500		5.46 ±0.22	0.641 ±0.026		19.7 ± 1.0	451 ± 13
300	0	100		1.05 ±0.02	.0472 ±0.0019		(b)	—
		300		1.11 ±0.02	.0463 ±0.0018			—
		500		1.15 ±0.02	.0421 ±0.0017			—
	500	100		1.18 ±0.04	0.0470 ±0.0024		30.4 ± 0.9	4790 ±100
		300		1.21 ±0.04	0.0485 ±0.0025		30.5 ± 1.2	4640 ±100
		500		1.20 ±0.04	0.0412 ±0.0021		31.9 ± 1.0	4840 ±100

Note:

a) For p ≥ 200 GeV/c the $e^{\pm}$'s produced in the target are lost before the CEDARs owing to synchrotron radiation in the bending magnets.

b) 300 GeV/c, p_T = 0 positives were not measured.

for the 100 mm target, which has the least reabsorption of the three targets measured and hence gives values close to those from a p-Be nucleus collision.

The agreement with the FNAL[10] results is in general good; however, direct comparison is difficult as no precise production angle was quoted there.

4.1.2 Change of particle ratios with p_T

Figure 7 shows the change of the particle ratios for p_T = 500 MeV/c relative to p_T = 0, plotted as a function of secondary momentum, again for the 100 mm target.

Although it would appear that both signs of particles tend to have the same behaviour at high and low momenta, there are strong differences at intermediate energies between positive and negative particles. In the framework of the Thermodynamic Model [H. Grote et al.[11]] of particle production, this difference could be attributed to the production of N^* resonances, of which the decays to KΛ or pπ alter the angular distributions away from the "inherent" behaviour of production from the "central" region where K^-'s and $\bar{p}$'s are produced.
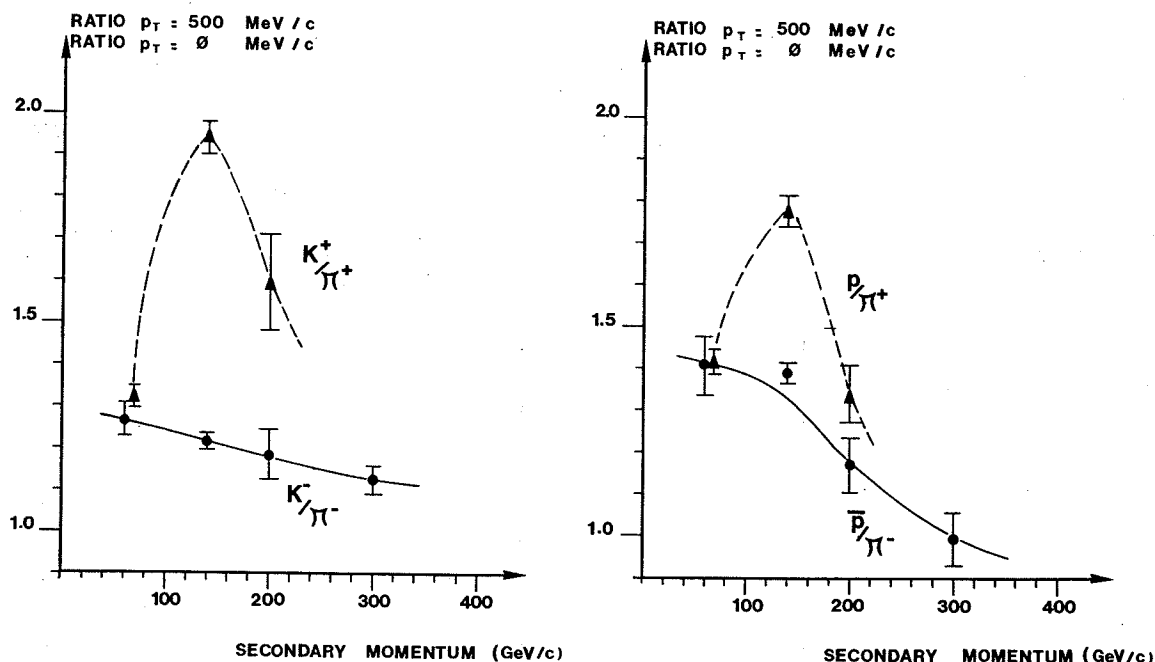

Fig. 7 Relative change of particle ratios between two values of p_T as a function of secondary momentum

4.1.3 Change of particle ratios with target length

As Table 4 indicates, the particle ratios are also a function of target length showing small but significant variations. Figure 8 shows the value of the ratios for the 500 mm target compared with the ratio of the 100 mm target as a function of secondary momentum, for p_T = 0 and 500 MeV/c.

For K^+/π^+, K^-/π^-, and $\bar{p}/\pi^-$ there is no variation with secondary momentum or p_T, and the values are in good agreement with a naive reabsorption model in which the produced secondaries
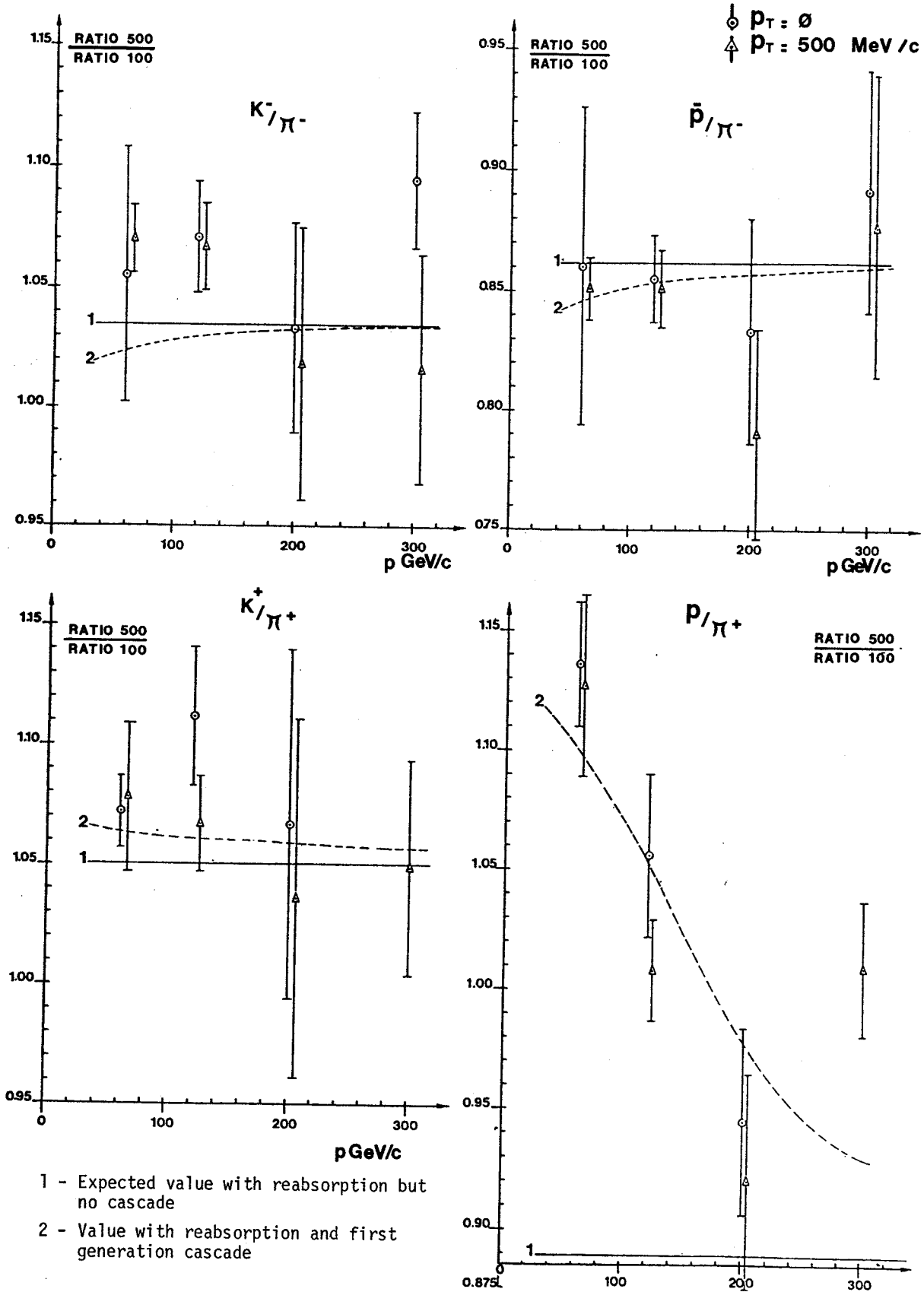
Fig. 8 Particle ratios for 500 mm target relative to the 100 mm target as a function of secondary momentum and for $p_T = 0$ and $p_T = 500$ MeV/c

are reabsorbed in the target without producing any more particles. This is a "no cascade" model and the variations with target length are due to the different absorption cross-sections of the different particles.

Using this model and the cross-sections from Ref. 9, averaged over 60, 200, and 280 GeV/c and interpolated to Be, gives the constant full line shown in the Fig. 8. The agreement is good except for p/π^+, where the variation with energy is very strong. Although the values tend towards this naive-model value at high energies, there is an inversion at lower energies, where more protons appear to be produced even though they are more strongly absorbed in the target than are the π^+'s.

As about 40% of produced secondary protons, which are still of high (200 to 400 GeV/c) energy, are reabsorbed in the 500 mm target, cascade effects will contribute significantly to p production at the lower momenta. The model was therefore extended to track one generation of tertiaries: secondary protons generated in a Monte Carlo program were made to reinteract with a cross-section derived from Ref. 9. The spectrum from these protons was then added to the initial spectrum with reabsorption. The result is shown by the dashed lines in Fig. 8.

The changes for K/π and $\bar{p}/\pi^-$ are small, as may be expected, but the effect on p/π^+ is very strong and gives a good explanation of the variation.

4.2 Absolute rates

Table 6 shows the absolute yields for hadrons from 40, 100, 300 and 500 mm Be targets. The measured values have been corrected to correspond to 100% of incident protons striking the target, and have also been adjusted for the 2.2 mm Be equivalent of the "target out" flux using the simple reabsorption model of the previous section. The particle contents values of the 100 mm target from Table 4 have been used as particle contents for the 40 mm target.

4.2.1 Flux as a function of target length

Figure 9 shows the ratio of total flux from the 500 mm (300 mm) target compared with the total flux from the 40 mm target, as a function of secondary momentum. If there were only reabsorption of the secondaries without cascade, then the expected ratios would be easy to calculate.

For the negative beam, we would expect a constant value at all energies as it is essentially 100% π^-'s and the absorption cross-section is constant. For positives, a variation with energy will occur owing to the changing p/π^+ ratio, these particles having very different absorption cross-sections. The result of this first-order calculation is shown by the dashed lines in Fig. 9.

It should be noted that the $e^\pm$ content has been subtracted out of the total flux because it has strong variations with target length that are characteristic of an electromagnetic cascade and not of a hadron cascade. Furthermore, the errors on individual points are much smaller than in Table 6, as they represent relative measurements taken over a short time and most of the systematic errors do not enter into this relative value.

Table 6

Absolute production rates of hadrons by 400 GeV/c protons incident on a beryllium target
Units are particles/incident proton µsr % dp/p
All numbers should be multiplied by 10^{-6}

p (GeV/c)	p_T (MeV/c)	Target length (mm)	π^-	K^-	$\bar{p}$	π^+	K^+	p
60	0	40	1.14 ± 0.07	0.093 ± 0.006	0.044 ± 0.003	1.64 ± 0.80	0.174 ± 0.011	0.372 ± 0.023
		100	2.73 ± 0.16	0.221 ± 0.015	0.106 ± 0.008	3.83 ± 0.23	0.405 ± 0.025	0.868 ± 0.054
		300	5.76 ± 0.35	0.516 ± 0.034	0.210 ± 0.016	7.96 ± 0.48	0.872 ± 0.053	1.93 ± 0.12
		500	6.70 ± 0.40	0.572 ± 0.038	0.224 ± 0.017	8.87 ± 0.54	1.008 ± 0.062	2.29 ± 0.14
	500	40	0.370 ± 0.021	0.C38 ± 0.002	0.020 ± 0.001	0.55 ± 0.03	0.076 ± 0.005	0.175 ± 0.011
		100	0.847 ± 0.049	0.087 ± 0.005	0.046 ± 0.003	1.26 ± 0.07	0.176 ± 0.011	0.403 ± 0.025
		300	1.83 ± 0.11	0.194 ± 0.011	0.093 ± 0.006	2.65 ± 0.15	0.395 ± 0.024	0.918 ± 0.058
		500	2.19 ± 0.13	0.241 ± 0.014	0.102 ± 0.006	2.94 ± 0.17	0.442 ± 0.027	1.06 ± 0.07
120	0	40	1.51 ± 0.09	0.099 ± 0.006	0.031 ± 0.002	4.41 ± 0.31	0.349 ± 0.024	2.82 ± 0.20
		100	3.43 ± 0.20	0.225 ± 0.013	0.071 ± 0.004	9.80 ± 0.68	0.775 ± 0.054	6.26 ± 0.44
		300	6.77 ± 0.41	0.463 ± 0.028	0.132 ± 0.008	19.0 ± 1.3	1.59 ± 0.11	12.5 ± 0.9
		500	7.60 ± 0.46	0.534 ± 0.032	0.135 ± 0.008	20.3 ± 1.4	1.79 ± 0.12	13.7 ± 1.0
	300	40	0.90 ± 0.05	0.068 ± 0.004	0.021 ± 0.0013	2.31 ± 0.16	0.273 ± 0.019	2.10 ± 0.14
		100	2.03 ± 0.12	0.155 ± 0.009	0.049 ± 0.003	5.16 ± 0.35	0.609 ± 0.041	4.68 ± 0.32
		300	4.00 ± 0.24	0.318 ± 0.019	0.090 ± 0.005	10.1 ± 0.7	1.22 ± 0.08	9.37 ± 0.64
		500	4.11 ± 0.25	0.330 ± 0.020	0.084 ± 0.005	11.3 ± 0.8	1.43 ± 0.10	10.5 ± 0.7
	500	40	0.54 ± 0.03	0.043 ± 0.003	0.016 ± 0.001	1.11 ± 0.08	0.171 ± 0.012	1.26 ± 0.09
		100	1.23 ± 0.07	0.098 ± 0.006	0.036 ± 0.002	2.52 ± 0.17	0.387 ± 0.026	2.86 ± 0.20
		300	2.51 ± 0.15	0.207 ± 0.012	0.067 ± 0.004	5.13 ± 0.35	0.81 ± 0.06	5.91 ± 0.41
		500	2.72 ± 0.16	0.232 ± 0.014	0.067 ± 0.004	5.72 ± 0.39	0.94 ± 0.06	6.55 ± 0.45

(contd)

Table 6 (contd)

p (GeV/c)	p_T (MeV/c)	Target length (mm)	π^-	K^-	$\bar{p}$	π^+	K^+	p
200	0	40	0.90 ± 0.05	0.041 ± 0.003	0.0062 ± 0.0004	–	–	–
		100	2.01 ± 0.12	0.091 ± 0.006	0.0139 ± 0.0008	6.55 ± 0.46	0.778 ± 0.059	23.9 ± 1.5
		300	3.92 ± 0.23	0.179 ± 0.012	0.0247 ± 0.0014	9.97 ± 0.70	1.23 ± 0.09	36.7 ± 2.4
		500	4.23 ± 0.25	0.197 ± 0.013	0.0244 ± 0.0014	14.23 ± 1.0	1.81 ± 0.14	49.1 ± 3.2
	500	40	0.298 ± 0.017	0.0160 ± 0.0011	0.0024 ± 0.0002	0.81 ± 0.05	0.154 ± 0.010	3.49 ± 0.24
		100	0.67 ± 0.04	0.0359 ± 0.0025	0.0054 ± 0.0003	1.80 ± 0.12	0.341 ± 0.022	8.79 ± 0.63
		300	–	–	–	3.64 ± 0.23	0.697 ± 0.045	16.9 ± 1.0
		500	1.50 ± 0.09	0.0820 ± 0.0058	0.0096 ± 0.0006	3.87 ± 0.25	0.760 ± 0.049	17.5 ± 1.0
300	0	40	0.110 ± 0.006	$(1.16\pm0.07)\times 10^{-3}$	$(0.52\pm0.03)\times 10^{-4}$	a)	–	–
		100	0.241 ± 0.014	$(2.53\pm0.15)\times 10^{-3}$	$(1.14\pm0.06)\times 10^{-4}$		–	–
		300	0.455 ± 0.026	$(5.06\pm0.30)\times 10^{-3}$	$(2.11\pm0.12)\times 10^{-4}$		–	–
		500	0.483 ± 0.027	$(5.56\pm0.33)\times 10^{-3}$	$(2.03\pm0.11)\times 10^{-4}$		–	–
	500	40	0.0488± 0.0027	$(0.576\pm.036)\times10^{-3}$	$(2.29\pm0.13)\times 10^{-5}$	0.203 ± 0.014	0.062 ± 0.004	9.73 ± 0.63
		100	0.0971± 0.0053	$(1.15\pm.08)\times10^{-3}$	$(4.56\pm0.28)\times 10^{-5}$	0.439 ± 0.030	0.134 ± 0.009	21.0 ± 1.4
		300	0.208 ± 0.012	$(2.52\pm.16)\times10^{-3}$	$(10.1\pm0.6)\times 10^{-5}$	0.848 ± 0.055	0.259 ± 0.018	39.5 ± 2.5
		500	0.218 ± 0.012	$(2.62\pm.17)\times10^{-3}$	$(9.00\pm0.51)\times 10^{-5}$	0.849 ± 0.056	0.269 ± 0.018	41.1 ± 2.6

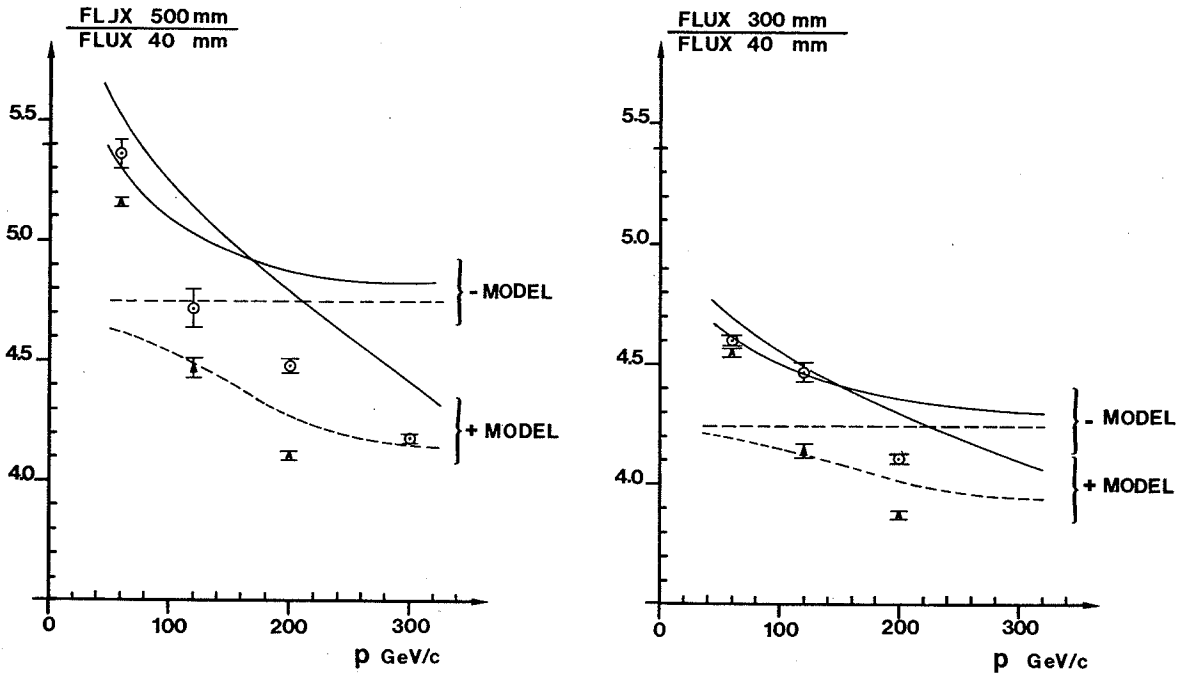a) 300 GeV/c, p_T = 0 positives were not measured.

Fig. 9 Variation of total flux with target length as a function of secondary momentum

It is clear that the simple reabsorption model is not a good one and that there are cascade effects visible at all energies, from about 3% at 200 GeV/c to about 25% at 60 GeV/c for the 500 mm target. As in Section 4.1.3, a rough cascade calculation was used to try to see if these effects are easily calculable. Using a Monte Carlo program, the reinteraction of the secondary protons was simulated, the tertiary flux produced by them was added to the straightforward secondary fluxes. As we are using ratios only, having the exact fluxes is not of great importance, and the formulae used in this Monte Carlo program were selected for ease of use only. They are shown along with the data in Fig. 10.

The result including this rough cascade effect is shown by the full lines in Fig. 9, and one sees that, although the shape of the curve is better, it is still not yet a reasonable fit to the data. In order to obtain a reasonable description with this rough model it would be necessary to increase the absorption cross-section by about 30% and increase the cascade contribution by about 40%. The absorption cross-sections measured at FNAL[9] for light elements are about 15% smaller than those measured at Serpukhov[12]; we have considered only secondary protons in the tertiary production, and there will be a contribution from the reabsorbed neutrons produced at high energies.
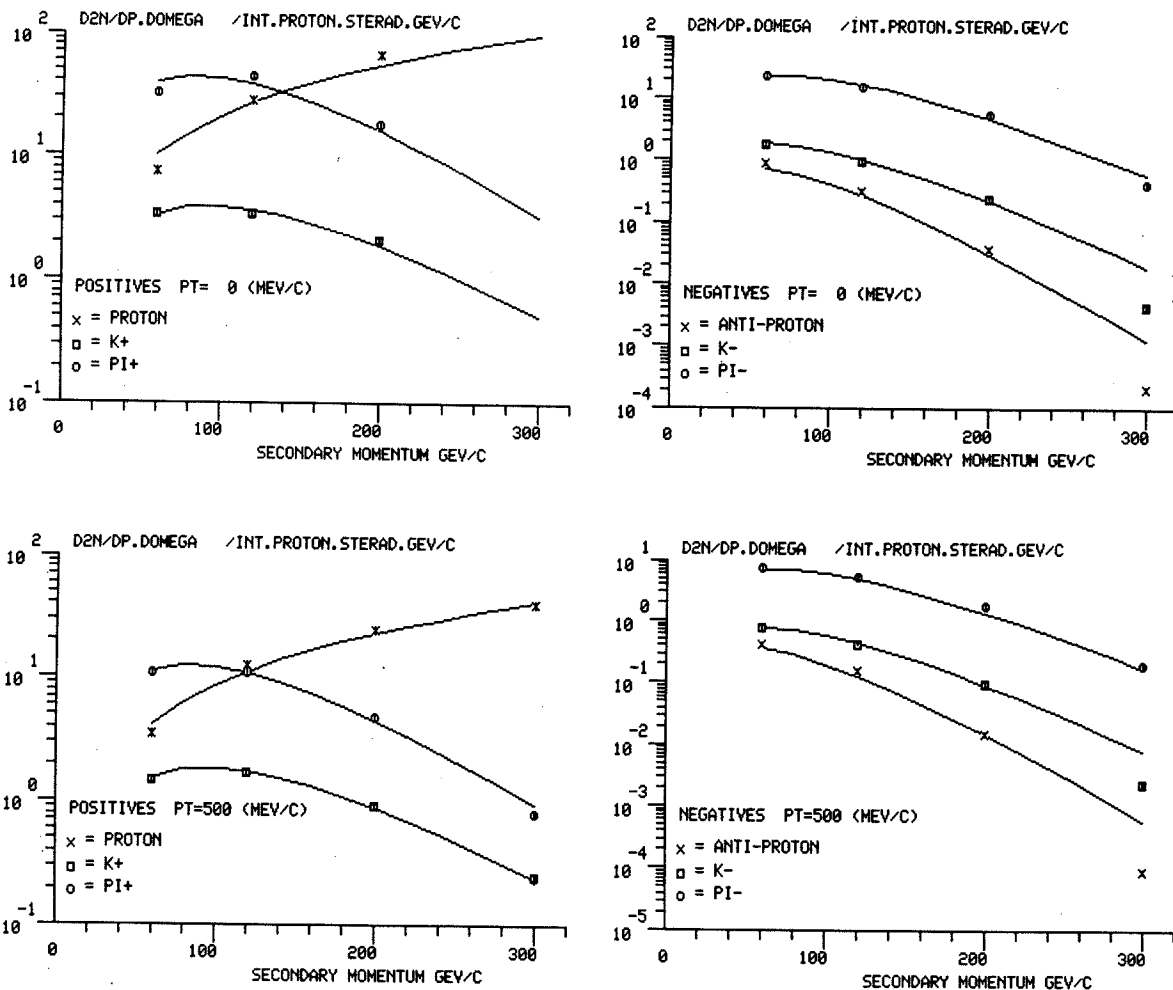
$$\frac{d^2N}{dpd\Omega} = A\left[\frac{B}{p_0} e^{-Bp/p_0}\right]\left[\frac{2Cp^2}{2\pi} e^{-C(p\theta)^2}\right] \qquad \frac{d^2N}{dpd\Omega} = A\left[\frac{(B+1)}{p_0}\left(\frac{p}{p_0}\right)^B\right]\left[\frac{2Cp^2}{2\pi} e^{-C(p\theta)^2}\right]$$

	A	B	C
π^+	1.2	9.5	5.0
π^-	0.8	11.5	5.0
K^+	0.16	8.5	3.0
K^-	0.10	13.0	3.5
$\bar{p}$	0.06	16.0	3.0

	A	B	C
p	0.8	-0.6	3.5

Fig. 10 Empirical formulae used to simulate the production results, compared to the measurements of p-Be collisions

4.2.2 *Comparison with the thermodynamic model*

Figures 11a and 11b show the absolute production from p-Be nucleus collisions extracted from the 40 mm target fluxes, where corrections for reabsorption are small (< 5%) and cascade effects are negligible.
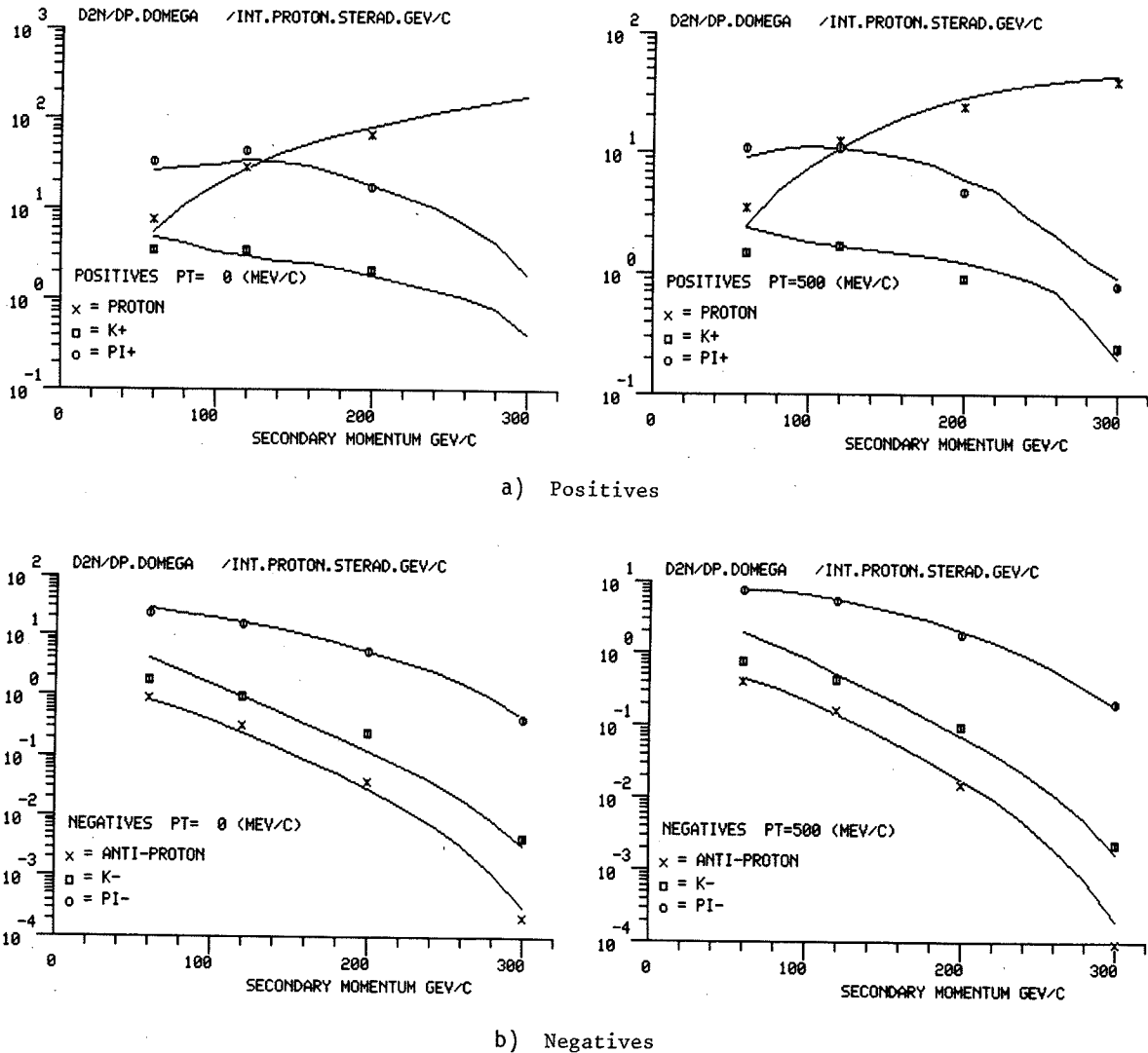
a) Positives

b) Negatives

Fig. 11 Production from p-Be collisions compared with the thermodynamic model

Superimposed on the measurements are some curves from the programs used to calculate production from the thermodynamic model. The constants used are for p-p collisions, and various over-all scaling factors were applied to make the absolute normalization more reasonable. No attempt at best fitting has been done, the following factors being applied to give reasonable results:

π^+, K^+, p	multiply model flux by 0.53,
π^-	multiply model flux by 0.45,
K^-, $\bar{p}$	multiply model flux by 0.64.

With these trivial modifications, which are what would be roughly expected in order to account for reabsorption in the Be-production nucleus, one sees that the global agreement is reasonable and that this model can confidently continue to be used in the various Monte Carlo ray-tracing programs into which it is embedded as the particle production generator.

Acknowledgements

A. Wetherell suggested this work to us, by pointing out its interest for the neutrino experiments, and took part in the measurements and subsequent discussions together with J. Allaby, D. Cundy, J. May, P. Monacelli, A. Navarro-Savoy, F. Navarria, J. Pattison, W. Venus and H. Wachsmuth.

Members of the CERN SPS/ABT, SPS/AOP, and HS/RA groups provided the SEM monitor foils and made the precise calibration of their sensitivity.

We are grateful to G.P. Ferri for his technical assistance during the installation and operation of the CEDARs.

REFERENCES

1) H. Wachsmuth, Proc. Neutrino Meeting, Geneva 1969 (CERN-69-28, Geneva, 1969), p. 33;
   D. Bloess, J.B.M. Pattison, G. Plass, D. Rusch, W. Venus and H.W. Wachsmuth, Nucl. Instr. Methods 91, 605 (1971).

2) SPS Experimenter's Handbook (1978), par. 7, p. 59.

3) C. Bovet, R. Maleyran, A. Placci and M. Placidi, IEEE Trans. Nucl. Sci. NS25, 572 (1978).

4) W. Kalbreier, W.C. Middelkoop and P. Sievers, Design principles of the target stations for the slow extracted proton beams of the SPS, CERN-Lab. II/BT/74-6 (October 1974).

5) A. Chapman-Hatchett, G. Cultrut, J. Dieperink, A. Fasso, W. Kalbreier, A. Müller, S. Peraire, M. Nielsen, A. Regelbrugge, G.R. Stevenson and D. Thomas, Calibration of the secondary emission monitors TBIU and TBID of the North Area target stations T2, T4 and T6 in TCC 2 for slow extracted protons of 400 GeV/c, SPS/ABT/Int. 79-1 (April 1979).

6) C. Bovet, A. Placci and M. Placidi, Paper in preparation.

7) W. Agoritsas and R.L. Witkover, Tests of SEC stability in high-flux proton beams, CERN/PS/EI 79-16 (1979).

8) J.H. Dieperink, The calibration and long-term stability of the SPS secondary emission monitors, SPS Improvement Report No. 121 (8 February 1978).

9) A.S. Carroll, I-H. Chiang, T.F. Kycia, K.K. Li, M.D. Marx, D.C. Rahm, W.F. Baker, D.P. Eartly, G. Giacomelli, A.M. Jonckheere, P.F.M. Koehler, P.O. Mazur, R. Rubinstein and O. Fackler, Phys. Lett. 80B, 319 (1979).

10) W.F. Baker, A.S. Carroll, I-H. Chiang, D.P. Eartly, O. Fackler, G. Giacomelli, A. Jonckheere, P.F.M. Koehler, T.F. Kycia, K.K. Li, M.D. Marx, P.O. Mazur, D.C. Rahm and R. Rubinstein, Fermilab report 78/79-Exp (1978).

11) See, for example, H. Grote, R. Hagedorn and J. Ranft, Atlas of particle spectra (CERN, Geneva, 1970).

12) J.V. Allaby, Yu.B. Bushnin, Yu.P. Gorin, S.P. Denisov, G. Giacomelli, A.N. Diddens, R.W. Dobinson, S.V. Donskov, A. Klovning, A.I. Petrukhin, Yu.D. Prokoshkin, C.A. Stahlbrandt, D.A. Stoyanova and R.S. Shuvalov, Soviet J. Nucl. Phys. 12, 295 (1971);
    S.P. Denisov, S.V. Donskov, Yu.P. Gorin, R.N. Krasnokutsky, A.I. Petrukhin, Yu.D. Prokoshkin and D.A. Stoyanova, Nucl. Phys. B61, 62 (1973).